Environmental Science & Technology

pubs.acs.org/est

Article

Dominant Contribution of NO_3 Radical to NO_3^- Formation during Heavy Haze Episodes: Insights from High-Time Resolution of Dual Isotopes $\Delta^{17}O$ and $\delta^{18}O$

Xinxin Feng, Yingjun Chen,* Shaofeng Chen, Yu Peng, Zeyu Liu, Minjun Jiang, Yanli Feng, Lina Wang, Li Li, and Jianmin Chen*

Cite This: *Environ. Sci. Technol.* 2023, 57, 20726−20735

Read Online

ACCESS | Metrics & More | Article Recommendations | Supporting Information

ABSTRACT: $\delta^{18}O$ is widely used to track nitrate (NO_3^-) formation but overlooks NO_3 radical reactions with hydrocarbons (HCs), particularly in heavily emitting hazes. This study introduces high-time resolution $\Delta^{17}O$-NO_3^- as a powerful tool to quantify NO_3^- formation during five hazes in three cities. Results show significant differences between $\Delta^{17}O$-NO_3^- and $\delta^{18}O$-NO_3^- in identifying NO_3^- formation. $\delta^{18}O$-NO_3^- results suggested N_2O_5 hydrolysis (62.0−88.4%) as the major pathway of NO_3^- formation, while $\Delta^{17}O$-NO_3^- shows the NO_3^- formation contributions of NO_2 + OH (17.7−66.3%), NO_3 + HC (10.8−49.6%), and N_2O_5 hydrolysis (22.9−33.3%), revealing significant NO_3 + HC contribution (41.7−56%) under severe pollution. Furthermore, NO_3^- formation varies with temperatures, NO_x oxidation rate (NOR), and pollution levels. Higher NO_2 + OH contribution and lower NO_3 + HC contribution were observed at higher temperatures, except for low NOR haze where higher NO_2 + OH contributions were observed at low temperatures ($T \leftarrow 10$ °C). This emphasizes the significance of NO_2 + OH in emission-dominated haze. Contributions of NO_2 + OH and NO_3 + HC relate to NOR as positive ($f_{P1} = 3.0*NOR^2 - 2.4*NOR + 0.8$) and negative ($f_{P2} = -2.3*NOR^2 + 1.8*NOR$) quadratic functions, respectively, with min/max values at NOR = 0.4. At mild pollution, NO_2 + OH (58.1 ± 22.2%) dominated NO_3^- formation, shifting to NO_3 + HC (35.5 ± 16.3%) during severe pollution. Additionally, high-time resolution $\Delta^{17}O$-NO_3^- reveals that morning−evening rush hours and high temperatures at noon promote the contributions of NO_3 + HC and NO_2 + OH, respectively. Our results suggested that the differences in the NO_3^- pathway are attributed to temperatures, NOR, and pollution levels. Furthermore, high-time resolution $\Delta^{17}O$-NO_3^- is vital for quantifying NO_3 + HC contribution during severe hazes.

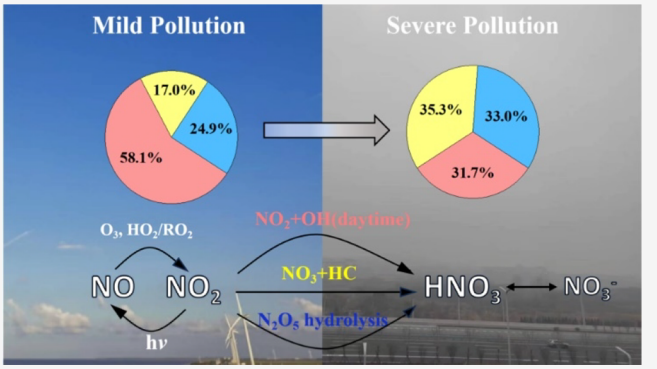

KEYWORDS: *nitrate, $\Delta^{17}O$-NO_3^-, formation pathways, haze episodes, NO_3 + HC*

1. INTRODUCTION

Most cities in China have experienced a dramatic increase in fine particulate matter ($PM_{2.5}$), especially during winter. Secondary inorganic aerosols (SIA: NH_4^+, NO_3^-, and SO_4^{2-}) dominate the composition of $PM_{2.5}$, contributing to 30−77% and driving the formation of hazes.[1,2] Recent studies have found a significant decrease in the mass concentration of SO_4^{2-} in $PM_{2.5}$, while the contribution of NO_3^- has become more prominent.[3−6] During severe haze episodes, the mass fractions of NO_3^- in $PM_{2.5}$ and SIA exceed 30 and 50%, respectively.[7,8] It is of great significance for understanding NO_3^- formation in heavy haze episodes to alleviate haze occurrence.

Atmospheric NO_3^- primarily originates from the oxidation of nitrogen oxides (NO_x = NO + NO_2). The conversion of NO_x to NO_3^- involves two main processes: the photochemical cycle of NO_x to form NO_2 in the atmosphere and the conversion of NO_2 into NO_3^- through three major pathways. These pathways include (i) daytime oxidation of NO_2 by the OH radical to produce HNO_3(g) (P1, NO_2 + OH), (ii) nighttime reaction of NO_2 with O_3 to form NO_3 radicals, which then react with hydrocarbons (HC, volatile organic compounds) to produce HNO_3(g) (P2, NO_3 + HC), and (iii) nighttime reaction of NO_3 with NO_2 to form N_2O_5, which undergoes heterogeneous reactions on wet aerosols to generate liquid-phase HNO_3 (P3, N_2O_5 hydrolysis).[9−11] The produced

Received: September 14, 2023
Revised: November 15, 2023
Accepted: November 16, 2023
Published: November 30, 2023

HNO_3 can directly react with alkaline gases (e.g., NH_3 and organic amines) to form atmospheric NO_3^-.[10] Different oxidants involved in NO_3^- formation are typically associated with varying degrees of oxygen isotopic fractionation $\varepsilon_{(NO2\rightarrow NO3-)}$.[12,13] For example, NO_3^- formed through reactions involving the OH radical (δ^{18}O-OH, −25 to 0‰) exhibits significantly lower δ^{18}O-NO_3^- values compared to those formed from ozone in the troposphere (δ^{18}O-O_3, 90−122‰), providing evidence for quantifying the contributions of different pathways to NO_3^- production.[14] Thus, the dual isotopes δ^{18}O and Δ^{17}O have been proven effective in tracing the formation pathways of NO_3^-.[3,12,14−19] Zhang et al.[14] used δ^{18}O-NO_3^- evidence to demonstrate that 60.9% of NO_3^- in the North China Plain during summer mainly originated from heterogeneous oxidation (N_2O_5 hydrolysis). Zong et al.[20] found that photochemistry (NO_2 + OH) contributed 58.0% of summertime NO_3^- loadings based on δ^{18}O-NO_3^- evidence. Although many studies have used δ^{18}O to investigate the formation pathways of NO_3^-, its application is restricted to certain regions due to its limitation in identifying only the NO_2 + OH and N_2O_5 hydrolysis pathways of NO_3^- formation. Unlike δ^{18}O, the oxygen-17 anomaly (Δ^{17}O) values represent mass-independent fractionation associated with ozone involvement ($\Delta^{17}O \neq 0‰$), and it has a more sensitive ability to identify the pathways of NO_3^- formation.[6] This method has been widely used in recent studies.[6,9,12,13,17,21,22] Zhang et al.[13] employed Δ^{17}O to reveal that NO_3 + HC and N_2O_5 hydrolysis were the dominant pathways for winter NO_3^- production in the urban area of Nanjing, with a significant contribution of 72% during nighttime. He et al.[9] also used Δ^{17}O-NO_3^- to show that NO_3 + HC and N_2O_5 hydrolysis were the major pathways, contributing 56−97% of NO_3^- during haze episodes in Beijing. Previous studies often used a single oxygen isotope (δ^{18}O or Δ^{17}O) to quantify the formation pathways of NO_3^-, finding that NO_2 + OH dominated in summer daytime, while the NO_3 + HC and N_2O_5 hydrolysis prevailed in winter nighttime.[3,13,20] However, other researchers have pointed out that NO_3 + HC shows significant contribution in the Beijing area of China, comparable to the other two pathways.[23] The inconsistency in these research results is due to the fact that many studies overlooked the NO_3 + HC contribution to NO_3^- yields using a single δ^{18}O. The deviation of the results will be even more pronounced, especially for heavily polluted regions in northern China during winter. Thus, it is crucial to re-evaluate the contribution of the NO_3 + HC to NO_3^- production using dual stable isotopes δ^{18}O and Δ^{17}O.

This study collected high-resolution haze samples from three cities in northern China, including Zibo in Shandong Province, Harbin in Heilongjiang Province, and Zhoukou in Henan Province. The high-time resolution dual isotopes δ^{18}O-NO_3^- and Δ^{17}O-NO_3^- were used synchronously to comprehensively quantify the mechanisms of NO_3^- formation. We evaluated the differences between Δ^{17}O and δ^{18}O in identifying the NO_3^- formation pathways. Results from the Δ^{17}O analysis suggested that the NO_3 + HC pathway is the major pathway for NO_3^- formation under severe pollution. Meanwhile, we explored the factors that impact NO_3^- formation during different hazes. In addition, high-time resolution Δ^{17}O provided new evidence and understanding of NO_3^- formation in the rapidly changing hazes and offered a comprehensive understanding for mitigating NO_3^- concentration in hazes.

2. MATERIALS AND METHODS

2.1. Sample Collection. A high-flow sampler (TE-6070, TISCH, U.S.) equipped with quartz filters was used to collect 159 sets of high-time resolution samples during five hazes from November 18, 2022, to February 9, 2023. The sampling sites were set in Zibo, Shandong Province; Harbin, Heilongjiang Province; and Zhoukou, Henan Province (Figure S1). Different sampling times were set for samples based on $PM_{2.5}$ concentration: 6 h ($PM_{2.5}$ < 75 $\mu g/m^3$) for mild pollution, 4 h (75 < $PM_{2.5}$ < 150 $\mu g/m^3$) for moderate pollution, and 2 h ($PM_{2.5}$ > 150 $\mu g/m^3$) for severe pollution. According to the sampling sites, five haze episodes were defined as ZB1, ZB2, HEB1, HEB2, and ZK, respectively. Detailed information about samples is shown in Table S1. Meteorological parameters such as temperature (T), humidity (RH), wind speed (WS), and pollutant concentrations, including $PM_{2.5}$, SO_2, NO_x, CO, and O_3, were obtained from the nearest environmental monitoring stations to the sampling sites.

2.2. Isotopic Analysis of δ^{18}O and Δ^{17}O for NO_3^-. A 30 cm^2 filter membrane was extracted with 20 mL of Milli-Q water for 30 min. The concentrations of water-soluble ions (Na^+, K^+, Ca^{2+}, Mg^{2+}, Cl^-, NO_3^-, SO_4^{2-}, and NH_4^+) were measured using an ion chromatograph (ICS 6000, Thermo Fisher, USA).[24,25] The dual oxygen isotopes (δ^{18}O and Δ^{17}O) were determined after converting NO_3^- (0.8 μgN) to N_2O through denitrification bacteria (ATCC13985).[26] The N_2O gas is catalytically decomposed to N_2 and O_2 by placing it in a gold tube at 800 °C.[3] The δ^{18}O and δ^{17}O of O_2 were measured using a stable isotope ratio mass spectrometer (MAT253, Thermo Fisher, USA). The Δ^{17}O of the sample nitrate was obtained using the formula $\Delta^{17}O = \delta^{17}O - 0.52 \times \delta^{18}O$.[27,28] The true isotope values of samples were obtained using the international standard samples USGS34 (Δ^{17}O = −0.1‰) and USGS35 (Δ^{17}O = +21.6‰). This method can measure oxygen isotope values of atmospheric samples with low NO_3^- concentration, with a repeatability precision of 0.1‰ for δ^{18}O and 0.3‰ for δ^{17}O (n = 10).

2.3. Evaluation of NO_3^- Formation Pathways by Δ^{17}O and δ^{18}O. The oxygen atom of ozone with Δ^{17}O is transferred to nitrate through various reactions during the formation of atmospheric NO_3^-, leading to the presence of Δ^{17}O signal in NO_3^-.[29,30] Different oxidants involved in the production of NO_3^- have distinct Δ^{17}O signals, as shown in eqs R1−R3.[29] By inputting the fractionation values [Δ^{17}O-NO_3^-] of the three oxidation pathways and the Δ^{17}O signal in NO_3^- into a Bayesian model (stable isotope analysis in R, SIAR),[31,32] the contributions of NO_3^- via NO_2 + OH (P1), NO_3 + HC (P2), and N_2O_5 hydrolysis (P3) can be quantified and defined as f_{P1}, f_{P2}, and f_{P3}, respectively, as shown in eqs R4 and R5.[29] Similarly, δ^{18}O can be used to evaluate the contributions of NO_2 + OH (P1) and N_2O_5 hydrolysis (P3) due to δ^{18}O-NO_3^- values with significant differences between the OH pathway (−25 to 0‰) and the N_2O_5 hydrolysis (90−122‰),[19,32−35] as shown in eqs R6 and R7:[19]

$$[\Delta^{17}O - NO_3^-]_{P1} = 2/3A \times \Delta^{17}O - O_3^* \quad (R1)$$

$$[\Delta^{17}O - NO_3^-]_{P2} = 2/3A \times \Delta^{17}O - O_3^* + 1/3\Delta^{17}O - O_3^* \quad (R2)$$

https://doi.org/10.1021/acs.est.3c07590
Environ. Sci. Technol. 2023, 57, 20726−20735

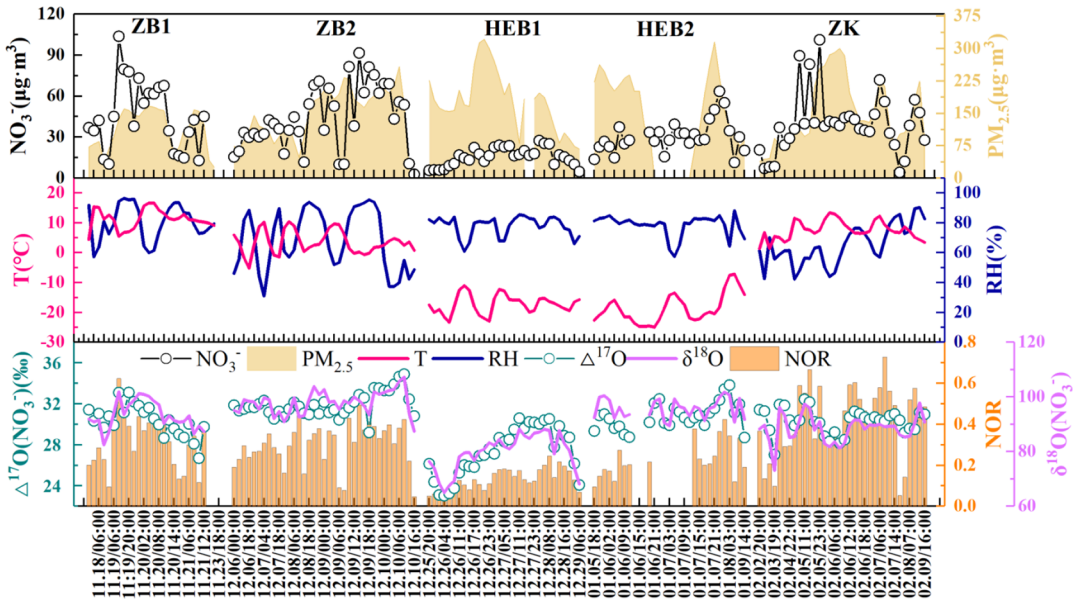

Figure 1. Time series of (1) concentrations of NO_3^- and $PM_{2.5}$, (2) T and RH, and (3) NOR and the values of $\Delta^{17}O\text{-}NO_3^-$ and $\delta^{18}O\text{-}NO_3^-$ in five hazes.

$$[\Delta^{17}O - NO_3^-]_{P3} = 2/3A \times \Delta^{17}O - O_3^* + 1/6\Delta^{17}O - O_3^* \quad (R3)$$

$$\Delta^{17}O - NO_3^- = [\Delta^{17}O - NO_3^-]_{P1} \times f_{P1} + [\Delta^{17}O - NO_3^-]_{P2} \times f_{P2} + [\Delta^{17}O - NO_3^-]_{P_3} \times f_{P3} \quad (R4)$$

$$f_{P1} + f_{P2} + f_{P3} = 1 \quad (R5)$$

$$\delta^{18}O - NO_3^- = f_{P1} \times [\delta^{18}O - NO_3^-]_{P1} + f_{P3} \times [\delta^{18}O - NO_3^-]_{P3} \quad (R6)$$

$$f_{P1} + f_{P3} = 1 \quad (R7)$$

Here, $\Delta^{17}O\text{-}O_3^*$ is used with a value of 39‰ ($\Delta^{17}O\text{-}O_3^* = 1.5\ \Delta^{17}O\text{-}O_{3bulk}$).[36,37] The A value represents the ratio of O_3 oxidation of NO relative to $HO_2\cdot$ and $RO_2\cdot$,[37] which depend on the concentrations of the corresponding oxidants.[38,39] The detailed calculation can be found in Text S1. Significant differences in the O_3 concentration and T concentration were observed during five hazes (Table S2), corresponding to different A values and fractionation values of oxidation pathways (Table S3). Lower fractionation values were observed for P1 (21.9 ± 4.0), P2 (35.4 ± 4.0), and P3 (28.7 ± 4.0) in ZB2 with low O_3 concentration compared to high O_3 concentration. Therefore, the corresponding fractionation values should be used to accurately calculate the NO_3^- formation pathways in different hazes. $[\delta^{18}O\text{-}NO_3^-]_{OH}$ and $[\delta^{18}O\text{-}NO_3^-]_{H2O}$ represent the $\delta^{18}O$ fractionation values produced by OH oxidation and N_2O_5 hydrolysis, respectively.

3. RESULTS AND DISCUSSION

3.1. Characteristics of NO_3^- in $PM_{2.5}$ and Oxygen Isotopes of NO_3^-. Figure 1 shows the time series of meteorological conditions (T and RH), concentrations of NO_3^- and $PM_{2.5}$, and values of $\Delta^{17}O\text{-}NO_3^-$ and $\delta^{18}O\text{-}NO_3^-$ in five hazes. The average values, listed in Table S2, show high RH (73.5 ± 14.4%) and low WS (1.3 ± 0.9m/s), which promoted the accumulation of pollutants and haze formation.[40−42] The $PM_{2.5}$ concentrations in HEB1 and HEB2 are much higher than that of ZB1, ZB2, and ZK, with values of 67.5−33.0 $\mu g\cdot m^3$ (179.3 ± 68.4 $\mu g\cdot m^3$) and 66.5−316.0 $\mu g\cdot m^3$ (210.4 ± 99.2 $\mu g\cdot m^3$), respectively. The $PM_{2.5}$ concentrations in five hazes are much higher than those of hazes in Shanghai.[43] It is worth noting that the NO_3^- concentration and proportion in HEB1 and HEB2 are much lower than those in other hazes (28.6−33.1%), with values of 15.7 ± 6.5 $\mu g\cdot m^3$ (9.7 ± 4.8%) and 30.6 ± 11.7 $\mu g\cdot m^3$ (17.2 ± 10.8%), respectively. Similarly, the NO_x oxidation rates (NOR, 0.18 ± 0.7) in Harbin hazes were significantly lower than in Zibo (0.29 ± 0.1) and Zhoukou (0.40 ± 0.2). This emphasizes that the increase in the NO_3^- concentration in $PM_{2.5}$ during Harbin hazes can be attributed to primary emission. Moreover, it was found that Harbin had lower temperatures (−7 to −25 °C) compared to Zibo (−5.2 to 16.7 °C) and Zhoukou (1.4 to 13.4 °C). This implies that a higher heating demand may be a possible reason leading to more primary emission in Harbin than in other cities.

The average values of $\Delta^{17}O\text{-}NO_3^-$ in ZB1, ZB2, HEB1, HEB2, and ZK are 30.4 ± 1.5, 31.9 ± 1.2, 27.3 ± 2.4, 30.8 ± 1.3, and 30.3 ± 1.2‰, respectively. These values are consistent with previous studies conducted in Beijing Winter of 2015 (27.8 ± 2.1 and 30.6 ± 1.8‰)[9,23] and Nanjing Winter (30.5‰).[13] However, they are higher than those reported in Taiwan Province (23.0 ± 5.0‰).[44] HEB1 had the lowest average $\Delta^{17}O\text{-}NO_3^-$ values among the five hazes, indicating a higher production of NO_3^- through the OH pathway (P1), resulting in more negative $\Delta^{17}O\text{-}NO_3^-$ values.[37] Conversely, higher average $\Delta^{17}O\text{-}NO_3^-$ values in the other hazes suggest a greater contribution from nocturnal formation pathways with enriched $\Delta^{17}O\text{-}NO_3^-$ values, such as NO_3 + HC and N_2O_5 hydrolysis.[37] The average values of $\delta^{18}O\text{-}NO_3^-$ in five hazes were 93.4 ± 5.1, 98.0 ± 4.2, 79.8 ± 6.6, 95.8 ± 3.5, and 88.4 ± 5.0‰, respectively. These values are significantly higher than those observed in the summer in the North China Plain (+73.7

https://doi.org/10.1021/acs.est.3c07590
Environ. Sci. Technol. 2023, 57, 20726−20735

± 7.8‰) and autumn in Southeast China cities (+71.8 ± 14.7‰).[17,20] This is due to seasonal differences in NO_3^- formation, with N_2O_5 hydrolysis dominating during the winter.[15,33] Similar to the $\Delta^{17}O$-NO_3^- results, HEB1 shows lower $\delta^{18}O$-NO_3^- values compared to those of the other hazes, indicating a prominent contribution of NO_2 + OH to NO_3^- yields.

3.2. Differences between $\Delta^{17}O$ and $\delta^{18}O$ in Identifying NO_3^- Formation Pathways. $\delta^{18}O$-NO_3^- and $\Delta^{17}O$-NO_3^- were used to quantify the contributions of P1(NO_2 + OH), P2 (NO_3 + HC), and P3 (N_2O_5 hydrolysis) to NO_3^- yields during five hazes. Significant differences were observed in the results of the two oxygen isotopes (Figure 2). The

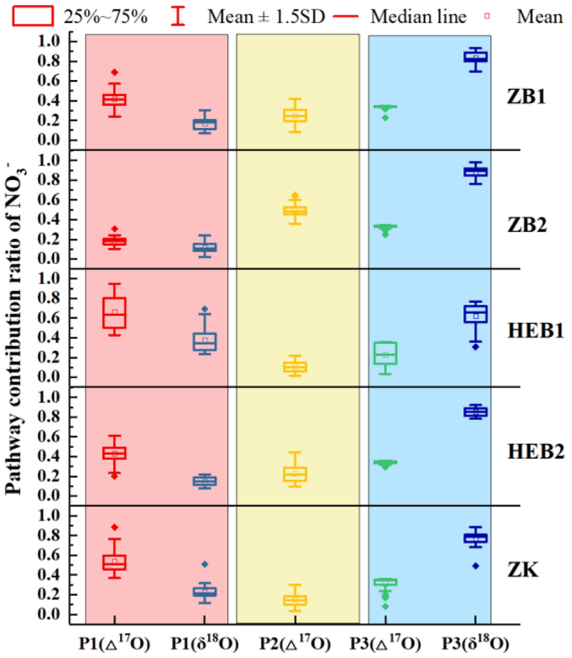

Figure 2. Formation contributions of NO_2 + OH (P1), NO_3 + HC (P2), and N_2O_5 hydrolysis (P3) to NO_3^- obtained by $\Delta^{17}O$ and $\delta^{18}O$ in five hazes.

$\Delta^{17}O$-NO_3^- results showed that NO_2 + OH was the major contributor for NO_3^- loadings in ZB1, HEB1, HEB2, and ZK, accounting for 41.8 ± 9.9, 66.3 ± 16.4, 43.2 ± 9.7, and 53.5 ± 11.6%, respectively. This finding highlights the importance of photochemical reactions in the formation of NO_3^- during hazes. Our results contradict the previous understanding that photochemical reactions dominate NO_3^- formation in summer, while liquid-phase heterogeneous reactions are more important in winter.[45] Particularly, the OH concentration is expected to be low in HEB1 due to its low temperature (−17.3 ± 3.1 °C) and O_3 concentration (18.4 ± 7.5 $\mu g \cdot m^3$).[46] However, it was found that the NO_2 + OH pathway contributed significantly to NO_3^- production in HEB1. One possible explanation is that the OH photochemical activity increases significantly with the rise in pollutant concentrations during hazes. Even with relatively low concentrations of OH, its photochemical activity becomes highly active due to the increased pollutant emissions.[45] On the other hand, the absence of high O_3 concentrations in winter haze may be due to its rapid consumption by the conversion of emitted NO to NO_2, as indicated by the highest NO_2 levels in HEB1 (76.8 ± 20.6 $\mu g \cdot m^3$, Table S2). Furthermore, NO_x exhibits the lowest oxidation rate (NOR, 0.13 ± 0.05) in HEB1, suggesting that the NO_2 + OH pathway has a greater advantage in generating NO_3^- in $PM_{2.5}$ under high emission conditions. Unlike summer, the O_3 concentration in winter hazes may not be suitable as an indicator of photochemical activity. In Zibo hazes, the NO_3 + HC pathway of ZB1 and ZB2 was found to be the significant contributor of NO_3^-, accounting for 24.9 ± 8.8 and 49.6 ± 6.1%, respectively. The lower O_3 concentration in Zibo hazes, as a precursor for NO_3, cannot explain the significant contribution of this pathway, but it is more likely attributed to the enhanced HC/DMS emission.[3] Based on the 72 h back trajectory of different hazes in Figure S2, the high concentration of DMS carried by clusters from the ocean may be the reason for the increased contribution of the NO_3 + HC/DMS pathway during the Zibo hazes. Moreover, P2 contributions in the other three hazes were also significant, especially for HEB2 (22.8 ± 9.2%). Unlike Zibo hazes, a large amount of HC emissions were measured in HEB2, as shown in Table S4, which lead to the prominent contribution of P2. Meanwhile, Fan et al. used $\Delta^{17}O$-NO_3^- to explore the differences in the formation pathways of NO_3^- at different pollution levels and found that the NO_3 + HC/N_2O_5+Cl^- pathway contributes 22−39% of NO_3^- production at low pollution levels and increases to 46−59% at high pollution levels.[3] He et al. reported $\Delta^{17}O$-NO_3^--constrained calculations suggesting that N_2O_5 + Cl^- and NO_3 + HC dominated 16−56% of NO_3^- production, emphasizing the non-ignorable role of both in the production of NO_3^- in Beijing haze.[9] Li et al. used $\Delta^{17}O$-NO_3^- to reveal the winter contribution of the NO_3 + HC/DMS pathway to NO_3^- production up to 30% in Qinyuan.[22] Wang et al. used $\Delta^{17}O$-NO_3^- to explore the formation pathway of nitrate in Guangzhou under different vertical altitude conditions and found that the contribution of the NO_3 + HC/DMS pathway to NO_3^- production increased from 12 to 25% with increasing altitude.[7] Wang et al. used $\Delta^{17}O$-NO_3^- to reveal that NO_3 + HC/DMS contributed 34% of NO_3^- formation in Beijing haze.[47] Thus, an increasing number of studies have pointed out that the reaction between NO_3 radicals and HC has a prominent contribution to NO_3^- production in haze. N_2O_5 hydrolysis (P3) was a secondary contribution pathway for NO_3^- yields in ZB1 (33.3 ± 2.3%), ZB2 (32.7 ± 2.3%), HEB1 (22.9 ± 10.9%), HEB2 (34.0 ± 1.7%), and ZK (31.4 ± 6.5%).

In contrast to $\Delta^{17}O$-NO_3^- results, $\delta^{18}O$-NO_3^- suggests that N_2O_5 hydrolysis (79.1 ± 12.2%) was the major pathway for NO_3^- yields in the five hazes. Due to the neglect of kinetic fractionation and the use of a wide range of $\delta^{18}O$-O_3 during the quantification of NO_3^- pathways,[32] there are significant uncertainties in the results of $\delta^{18}O$-NO_3^- for identifying NO_3^- formation pathways. In comparison, the unique $\Delta^{17}O$-NO_3^- signal resulting from ozone reactions enhances the sensitivity and accuracy in assessing the relationship between NO_3^- and atmospheric chemistry. For the uncertainty of $\Delta^{17}O$ analysis results, it can be found in Text S1 that accurate A values and $\Delta^{17}O$-O_3* are key to ensuring the accuracy of the analysis results. In this study, the A value at the corresponding time can be obtained based on high-resolution haze samples, which to some extent reduces result uncertainty. Moreover, the $\Delta^{17}O$-O_3* value in this study is consistent with that of previous studies.[36,37] Thus, $\Delta^{17}O$-NO_3^- is better suited for evaluating NO_3^- formation pathways in complex atmospheric environments.[47] Compared to $\Delta^{17}O$-NO_3^- results, the contributions of N_2O_5 hydrolysis from $\delta^{18}O$-NO_3^- were overestimated by

https://doi.org/10.1021/acs.est.3c07590
Environ. Sci. Technol. 2023, 57, 20726−20735

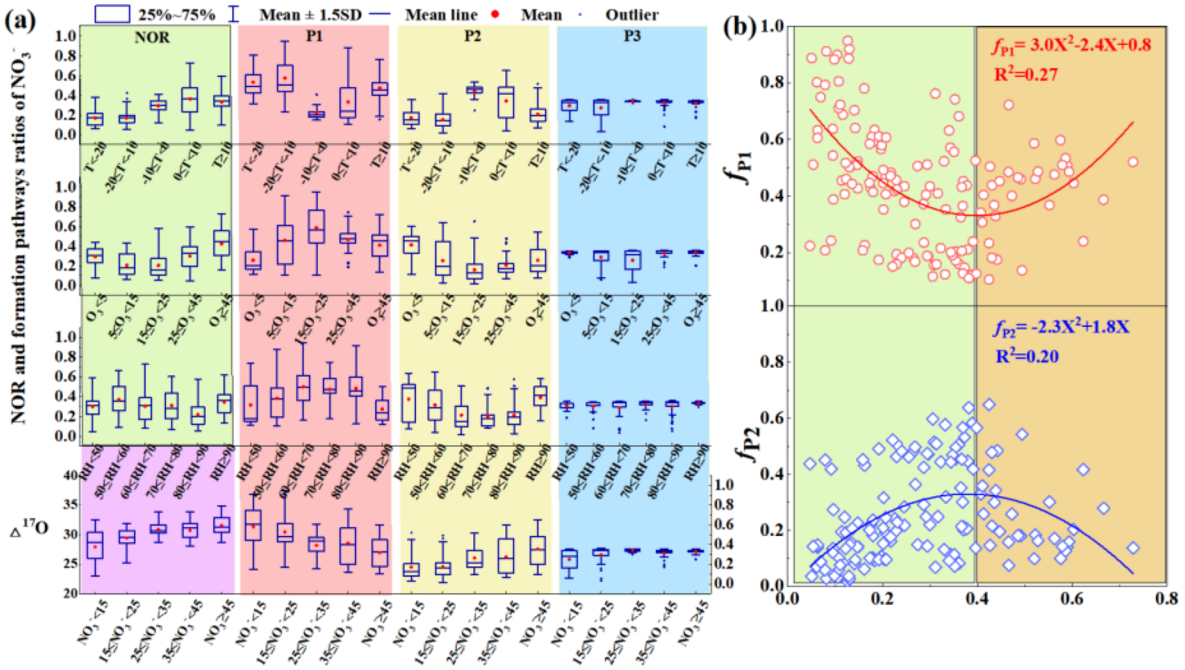

Figure 3. Influence of (a) *T*, RH, O_3, and pollution levels and (b) NOR on NO_3^- formation pathways.

49.9 ± 6.3, 55.7 ± 6.5, 39.1 ± 12.4, 51.0 ± 4.3, and 44.6 ± 4.1% in ZB1, ZB2, HEB1, HEB2, and ZK, respectively. Correspondingly, NO_2 + OH contributions to NO_3^- yields in ZB1, ZB2, HEB1, HEB2, and ZK were significantly underestimated by $\delta^{18}O$, reaching 25.0, 6.1, 28.3, 28.2, and 30.5%, respectively. It is important to note that 10.8−49.6% of NO_3^- produced from NO_3 + HC (P2) in the five hazes is disregarded. This leads to an underestimation of HC contribution to NO_3^- and an increase in uncertainty when predicting NO_3^- concentrations. Therefore, $\Delta^{17}O$ as a more powerful tool can provide a more comprehensive understanding of the pathways for the formation of NO_3^- in hazes. The discussion mainly focuses on the $\Delta^{17}O$ analysis results.

3.3. Impact Factors of NO_3^- Formation Pathways. Figure 3 shows the relationships between meteorological conditions (*T*, RH, NOR, and O_3), pollution levels, and NOR and NO_3^- formation. As the temperature increases, higher contributions of NO_2 + OH and lower contributions of NO_3 + HC were observed. This can be attributed to enhanced photolysis and reduced heating demand. However, in cases of Harbin hazes with low NOR, higher NO_2 + OH contributions are observed at relatively low temperatures ($T \leftarrow 10$ °C) compared to high temperature ($-10 \le T < 10$ °C) in other hazes. Figure 3b shows a positive quadratic relationship (f_{P1} = 3.0*NOR^2 − 2.4*NOR + 0.8) between NO_2 + OH and NOR, where the contribution of NO_2 + OH initially decreases and then increases with increasing NOR values. This trend can be observed in Harbin hazes, where the highest contribution of NO_2 + OH corresponds to lower NOR. Similarly, NOR reaches its lowest value when the O_3 concentration is between 15 and 25 $\mu g \cdot m^3$, corresponding to the maximum contribution of NO_2 + OH. This finding highlights the significance of the OH pathway in NO_3^- formation driven by emissions. Furthermore, a high RH typically promotes the formation of NO_3^-. However, our study reveals that the relationship between NOR and RH does not consistently show a positive trend. The impact of N_2O_5 hydrolysis on NO_3^- formation remains relatively stable as *T* and RH increase, indicating that N_2O_5 hydrolysis is not the dominant pathway of NO_3^- yields in high RH hazes (average values >73.5%). The influence of RH on NO_3^- formation is relatively complex, as the contributions of both NO_2 + OH and NO_3 + HC exhibit diversity with increasing RH. Further analysis reveals a negative quadratic relationship between NOR and NO_3 + HC (f_{P2} = −2.3*NOR^2 + 1.8*NOR, Figure 3b). The contribution of NO_3 + HC to NO_3^- yields first increases and then decreases as NOR increases, reaching its maximum at NOR = 0.4. Due to the quadratic relationships between NOR and NO_3^- formation pathways (NO_2 + OH and NO_3 + HC), NOR may be a more sensitive indicator than meteorological conditions for reflecting the formation pathways of NO_3^- in hazes.

In addition, the formation pathways of NO_3^- show differences at different pollution levels. The $\Delta^{17}O$-NO_3^- values increase from 28 ± 2.8‰ (NO_3^- < 15 $\mu g \cdot m^3$) to 31.6 ± 1.5‰ (NO_3^- ≥ 45 $\mu g \cdot m^3$). Higher $\Delta^{17}O$ values in the severe pollution level indicate prominent contributions of NO_3 + HC and N_2O_5 hydrolysis to NO_3^- formation due to the distinctive high $\Delta^{17}O$ signal of O_3.[3,28,37] In Figure 3a, it has been found that the contribution of NO_3 + HC to NO_3^- formation increases from 17.0 ± 14.2% in NO_3^- < 15 $\mu g \cdot m^3$ to 35.3 ± 16.3% in NO_3^- ≥ 45 $\mu g \cdot m^3$, which is associated with increased HC emissions under severe pollution level. As shown in Figures S3 and S4, the increase in the P2 contribution is accompanied by an increase in the HC concentration, such as oxygenated/intermediate volatile organic compounds (O/IVOCs). For example, the OVOC concentration increased from 18.9 $\mu g \cdot m^{-3}$ in low P2 contribution to 30.6 $\mu g \cdot m^{-3}$ in high P2 contribution. Meanwhile, the concentration of IVOCs is 1 order of magnitude higher than that of OVOCs in the five hazes. The concentration of IVOCs from 45.5 $\mu g \cdot m^{-3}$ in the low contribution of the NO_3 + HC pathway increases to 55.4 $\mu g \cdot m^{-3}$ in the high contribution of the NO_3 + HC pathway contribution. The relationships between the O/IVOCs and the

https://doi.org/10.1021/acs.est.3c07590
Environ. Sci. Technol. 2023, 57, 20726−20735

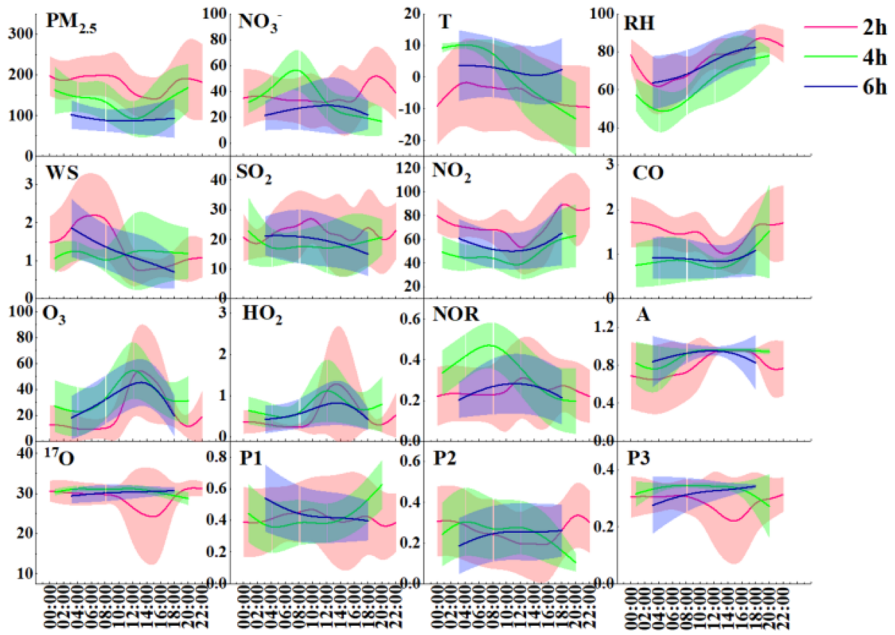

Figure 4. Diurnal variations curves of 2, 4, and 6 h, including meteorological conditions, gaseous precursors, and NO_3^- formation pathways.

NO_3 + HC pathway contribution can be found in Text S2. In addition, it is difficult to distinguish the contributions of the NO_3 + HC pathway and the N_2O_5 + Cl^- pathway by $\Delta^{17}O$-NO_3^- due to the same fingerprint feature between the two paths. According to the relationship between NO_3 + HC pathway contribution and Cl^- concentration in five haze episodes (Figure S5), we found that Cl^- concentration in five haze episodes was 4.7 ± 2.9 $\mu g \cdot m^{-3}$ in low P2 contribution, while Cl^- concentration only increased by 2.8 $\mu g \cdot m^{-3}$ in high P2 contribution. Compared to the other HC species, the lower growth rate of the Cl^- concentration showed that it is not the main pathway of NO_3^- formation. Thus, the increased HC emission (O/IVOCs) is an important reason for the increase in NO_3 + HC pathway contribution under different pollution levels. Moreover, the contribution of N_2O_5 hydrolysis shows a slow increasing trend from 24.9 ± 10.2% (mild pollution) to 33.0 ± 2.4% (severe pollution). Conversely, the lower $\Delta^{17}O$ values in the mild pollution level suggest the importance contribution of NO_2 + OH to NO_3^- production, which decreases rapidly from 58.1 ± 22.2% at mild pollution to 31.7 ± 14.8% at severe pollution. A possible explanation could be that increased pollution has weakened solar radiation, leading to a reduction in the number of OH photochemical reactions. Our study shows that NO_2 + OH (58.1 ± 22.2%) is the main pathway during the mild pollution level, while NO_3 + HC becomes the dominant pathway for NO_3^- formation (35.5 ± 16.3%) at severe pollution level. The significant role of NO_3 + HC in the formation of NO_3^- during severe pollution levels of hazes should be of concern. It highlights the importance of strict control of HC emissions to effectively alleviate the explosive growth of the NO_3^- concentration in haze.

3.4. Diurnal Variation of NO_3^- Formation Pathways. The curves of 2, 4, and 6 h in Figure 4 represent the diurnal variation characteristics of different components under severe pollution ($PM_{2.5}$ > 150 $\mu g/m^3$), moderate pollution (75 < $PM_{2.5}$ < 150 $\mu g/m^3$), and mild pollution ($PM_{2.5}$ < 75 $\mu g/m^3$), respectively. Additionally, they also reflect the ability of samples with different time resolutions to identify the NO_3^- formation. The diurnal variations of $PM_{2.5}$, CO, and NO_2 show good consistency, with higher concentrations at night compared to daytime. Their concentrations reach maximum values at peak hours and a minimum at noon in the 2 h curve (severe pollution). Similarly, the contribution of NO_3^- from NO_3 + HC follows the trends observed in the 2 h curve, with significantly higher contributions during nighttime and morning−evening peak hours compared to daytime and at noon. This is attributed to increased vehicle emissions during peak hours and reduced accumulation of pollutants with the increase in the daytime boundary layer. Furthermore, RH and *T* exhibit opposite diurnal variations. *T* is higher during the day, peaking at noon, which corresponds to the highest concentrations of O_3 and HO_2 (Text S1) at noon (14:00).[28,48] This is because intense light promotes the production of aluminating elements such as O_3 and HO_2. Meanwhile, NOR and the contribution of NO_2 + OH reach their maximum at noon in the 2 h curve, indicating a prominent contribution of NO_2 + OH during the daytime at noon. Higher *A* values were also observed during the day, peaking at noon with a range from 0.96 to 0.97. This leads to greater fractionation values produced by three pathways: P1 (25.5‰), P2 (39.1‰), and P3 (32.4‰). Moreover, the $\Delta^{17}O$ value (26.2‰) at noon during severe pollution is closer to the fractionation value produced by the NO_2 + OH pathway, suggesting the higher photochemical contribution to NO_3^- production at noon. However, *A* values show larger variations during the night of severe pollution, with a minimum value of 0.74, corresponding to lower fractionation values of P1 (19.8‰), P2 (33.3‰), and P3 (26.5‰) pathways. At this time, the $\Delta^{17}O$ value (30.2‰) is closer to the fractionation values of P2 and P3 pathways, providing evidence that the NO_3 + HC and N_2O_5 pathways dominate the nighttime formation of NO_3^-.

In addition, it was found that the diurnal variation trends of each component tend to stabilize as the time resolution decreases from 2 to 6 h, even approaching a straight line. For example, no obvious peak hours can be observed in the diurnal variation of $PM_{2.5}$, CO, NO_2, and SO_2 in the 4 and 6 h curves, weakening the information from the emission source. Moreover, it was found that the contributions of NO_3 + HC and

https://doi.org/10.1021/acs.est.3c07590
Environ. Sci. Technol. 2023, 57, 20726−20735

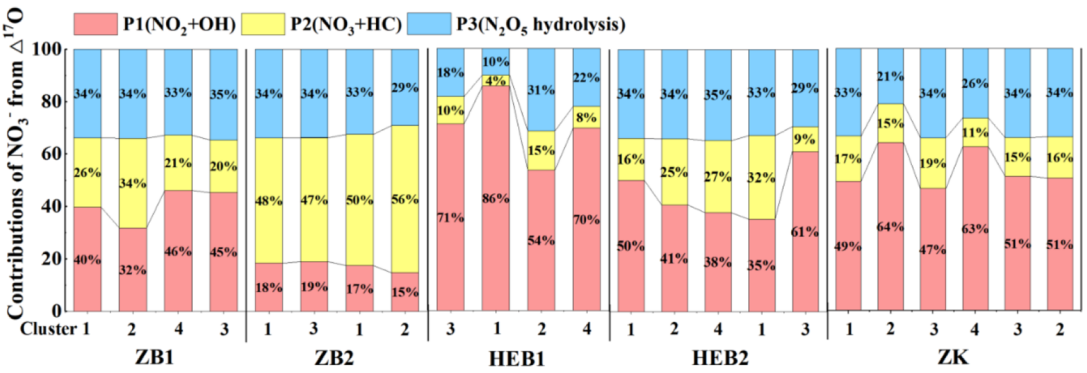

Figure 5. Formation pathways of NO_3^- under different hazes and clusters.

N_2O_5 hydrolysis were mainly active to NO_3^- formation during the day than at night in the 4 and 6 h curves. The diurnal variation of NO_2 + OH shows higher levels at night than during the daytime. Those results from low-time-resolution samples were obviously contrary to those of high-time-resolution samples. A possible explanation is that the low-resolution $\Delta^{17}O$ signal weakens the detailed information in evaluating the pathways of NO_3^- formation, leading to considerable uncertainty in the results. Our results emphasize the necessity of high-time-resolution samples to ensure result accuracy.

3.5. Formation Pathways of NO_3^- under Different Hazes and Clusters. Figure 5 displays the contribution ratios of NO_3^- formation pathways in different hazes and clusters obtained by $\Delta^{17}O$. The 72 h back trajectory and the composition characteristic of each cluster in five hazes are shown in Figures S2 and S6, respectively. Local pollution cluster 2, with a higher NO_3^- concentration (68.9 $\mu g/m^3$) than marine clusters 1, 3, and 4 (0.5−43.0 $\mu g/m^3$), leads to the haze formation of ZB1 (Figures S2 and S6). Furthermore, it is found that NO_2 + OH contributed 40−46% of NO_3^- in marine clusters 1, 3, and 4. In contrast, local pollution cluster 2 with higher HC concentration (OVOCs, 29.4 $\mu g/m^3$) leads to higher NO_3 + HC contribution up to 34% of NO_3^- production compared to marine clusters (NO_3 + HC, 20−26%). Especially during the peak pollution period of ZB1, the contribution of NO_3 + HC to NO_3^- formation can reach 41.7% (Figure S7). Moreover, ZB2 is mainly driven by local clusters 1 and 3, where the contribution of NO_3 + HC to NO_3^- formation consistently remains dominant (47−56%), followed by N_2O_5 hydrolysis (29−34%) and NO_2 + OH (15−19%). ZB2 is successively influenced by clusters 1, 3, 1, and 2, with corresponding NO_3^- concentrations of 17.6, 32.3, 57.9, and 30.7 $\mu g/m^3$, respectively (Figure S6). It was found that the contribution of NO_3 + HC to NO_3^- yields also increases from 48 to 56% with the increase in HC emission (OVOCs, from 13.8 to 31.1 $\mu g/m^3$). These results confirm that NO_3 + HC plays a non-negligible role in NO_3^- formation, particularly in severe pollution level, as shown in Figure 3b.

HEB1 is influenced by clusters 1 and 3 from Russia, as well as clusters 2 and 4 from Heilongjiang Province. As shown in Figure S6, all clusters show high concentrations of $PM_{2.5}$ (84.3−248.6 $\mu g/m^3$), SO_2 (23.8−36.5 $\mu g/m^3$), NO_2 (47.7−101.9 $\mu g/m^3$), RH (72.2−81.6%), and low NOR (0.07−0.17) and NO_3^- concentration (7.3−20.5 $\mu g/m^3$). The $\Delta^{17}O$ values in HEB1 (23.9−29.4‰) are significantly lower than in other hazes, suggesting that NO_2 + OH (54−86%) is the main pathway for NO_3^- formation in HEB1. This finding contradicts the lower OH concentration due to low temperature (−16.2 to −29.9 °C). We speculate that the high HC concentration under high emissions and low NOR may contribute to the prominent role of NO_2 + OH (Figure S6).[49,50] Additionally, the relationships between the contributions of NO_2 + OH and NO_3 + HC and NOR were consistent with Figure 3b. For example, an increase in NOR from cluster 1 (0.11) to cluster 2 (0.17) corresponds to a decrease in the NO_2 + OH contribution from 86 to 54%. Similarly, a decrease in NOR from 0.17 in cluster 2 to 0.14 in cluster 4 corresponds to an increase in NO_2 + OH contribution from 54 to 70%. Compared to HEB1, HEB2 is influenced by the northwest clusters 1, 2, 3, and 4, with significantly higher NOR values (0.18−0.33) corresponding to the increased NO_3 + HC contributions and decreased NO_2 + OH contribution (35−41%). Clusters 1 (0.18) and 3 (0.19) in HEB2 with lower NOR exhibit prominent contributions from NO_2 + OH (50 and 61%), while clusters 2, 4, and 1 show a decrease in NO_2 + OH contribution and an increase in NO_3 + HC contribution with increasing NOR. Compared to HEB1, ZK showed higher temperature (3.2−10.1 °C), RH (55.6−87.6%), and O_3 concentrations (44.1−72.5 $\mu g/m^3$), corresponding to higher OH photochemical activity and higher contributions from NO_2 + OH (47−64%). N_2O_5 hydrolysis acts as a secondary pathway of NO_3^-, with the minimum (21%) and maximum (34%) contributions observed at low RH (cluster 2, 57.3%) and high RH (cluster 2, 87.6%), respectively. Moreover, compared to HEB2, ZK haze shows lower contributions from NO_3 + HC (11−19%) due to the lower emissions of HC during the Chinese Lantern Festival (Table S4 and Figure S6). Furthermore, compared to the analysis results of $\delta^{18}O$-NO_3^- in Figure S8, this study emphasizes the necessity of using $\Delta^{17}O$ to constrain the pathways of NO_3^- formation during severe haze pollution, as its sensitivity is suitable for complex atmospheric environments.

4. IMPLICATION

This study employs high-time resolution dual-isotope $\Delta^{17}O$ and $\delta^{18}O$ to investigate NO_3^- formation in different hazes in cities of northern China. The results of $\delta^{18}O$ overlook NO_3 + HC contribution, while $\Delta^{17}O$ provides a more comprehensive and sensitive constraint on NO_3^- formation. Significant differences of the formation pathways of NO_3^- in different hazes can be observed due to the influence of various factors, such as NOR, temperature, and pollution levels. NOR and pollution levels are more effective indicators than meteorological conditions to reflect the formation of NO_3^- in hazes. For example, in emission-dominated hazes, NO_2 + OH is the

https://doi.org/10.1021/acs.est.3c07590
Environ. Sci. Technol. 2023, 57, 20726−20735

dominant pathway for the NO_3^- formation. However, the contribution of NO_3 + HC increases with increasing NOR and pollution levels, reaching its maximum value at NOR = 0.4 and severe pollution levels. Utilizing $\Delta^{17}O$ is crucial for accurately quantifying the formation pathways of NO_3^-, especially during severe hazes. Additionally, there are uncertainties in the evaluation process of NO_3^- formation pathways using $\Delta^{17}O$. First, the *A* values were obtained using empirical formulas due to limited monitoring of radical concentrations (HO_2/RO_2). To reduce the uncertainties associated with *A* values, efforts can be made to strengthen the monitoring of radical concentrations and directly measure the $\Delta^{17}O$-NO_2 end-member value. Second, we found that the $\Delta^{17}O$ signal characteristics are lower in emission-dominated hazes. Therefore, it is necessary to better evaluate the influence of emission sources on the $\Delta^{17}O$-NO_3^- values in environmental samples to obtain more accurate results on the NO_3^- formation. Finally, the $\Delta^{17}O$ signal can be incorporated into air quality models to simulate and predict NO_3^- concentrations in the future.

■ ASSOCIATED CONTENT

Supporting Information

The Supporting Information is available free of charge at https://pubs.acs.org/doi/10.1021/acs.est.3c07590.

Additional information regarding the evaluation of *A* values and fractional values of [$\Delta^{17}O$-NO_3^-] can be found in Text S1 and Table S3; sample information, sampling sites, 72 h back trajectories, relationships between OVOC, IVOCs, Cl^-, and NO_3 + HC pathway contribution, and component characteristic of five hazes shown in Table S1 and Figures S1−S6, respectively; time series of the contribution ratios of NO_3^- formation pathways obtained by $\Delta^{17}O$-NO_3^- and formation pathways of NO_3^- under different clusters from $\delta^{18}O$-NO_3^- shown in Figures S7 and S8; average values of $PM_{2.5}$, its components, and oxygen isotopes during the five hazes listed in Table S2; detailed information about HC species (O/IVOCs) in Text S2 and Table S4 (PDF)

■ AUTHOR INFORMATION

Corresponding Authors

Yingjun Chen − *Shanghai Key Laboratory of Atmospheric Particle Pollution and Prevention (LAP^3), Department of Environmental Science and Engineering, Fudan University, Shanghai 200433, P.R. China; Shanghai Institute of Pollution Control and Ecological Security, Shanghai 200092, China;* orcid.org/0000-0002-4784-8282; Email: yjchenfd@fudan.edu.cn

Jianmin Chen − *Shanghai Key Laboratory of Atmospheric Particle Pollution and Prevention (LAP^3), Department of Environmental Science and Engineering, Fudan University, Shanghai 200433, P.R. China;* orcid.org/0000-0001-5859-3070; Email: jmchen@fudan.edu.cn

Authors

Xinxin Feng − *Shanghai Key Laboratory of Atmospheric Particle Pollution and Prevention (LAP^3), Department of Environmental Science and Engineering, Fudan University, Shanghai 200433, P.R. China*

Shaofeng Chen − *Shanghai Key Laboratory of Atmospheric Particle Pollution and Prevention (LAP^3), Department of Environmental Science and Engineering, Fudan University, Shanghai 200433, P.R. China*

Yu Peng − *Shanghai Key Laboratory of Atmospheric Particle Pollution and Prevention (LAP^3), Department of Environmental Science and Engineering, Fudan University, Shanghai 200433, P.R. China*

Zeyu Liu − *Shanghai Key Laboratory of Atmospheric Particle Pollution and Prevention (LAP^3), Department of Environmental Science and Engineering, Fudan University, Shanghai 200433, P.R. China;* orcid.org/0000-0001-9138-4465

Minjun Jiang − *Institute of Environmental Pollution and Health, School of Environmental and Chemical Engineering, Shanghai University, Shanghai 200444, China*

Yanli Feng − *Institute of Environmental Pollution and Health, School of Environmental and Chemical Engineering, Shanghai University, Shanghai 200444, China*

Lina Wang − *Shanghai Key Laboratory of Atmospheric Particle Pollution and Prevention (LAP^3), Department of Environmental Science and Engineering, Fudan University, Shanghai 200433, P.R. China;* orcid.org/0000-0002-1474-9173

Li Li − *Institute of Environmental Pollution and Health, School of Environmental and Chemical Engineering, Shanghai University, Shanghai 200444, China*

Complete contact information is available at: https://pubs.acs.org/10.1021/acs.est.3c07590

Author Contributions

Y.C. designed this research. X.F. analyzed the data and wrote the original manuscript. S.C., Y.P., Z.L., and M.J. conducted the field work and laboratory experiments. L.L. provided the auxiliary data of Zibo haze. Y.F., L.W., and J.C. provided writing suggestions. All authors have given approval to the final version of the manuscript.

Notes

The authors declare no competing financial interest.

■ ACKNOWLEDGMENTS

This work was supported by the National Natural Science Foundation of China (nos. 91744203 and 42177086).

■ REFERENCES

(1) Huang, R. J.; Zhang, Y.; Bozzetti, C.; Ho, K. F.; Cao, J. J.; Han, Y.; Daellenbach, K. R.; Slowik, J. G.; Platt, S. M.; Canonaco, F.; Zotter, P.; Wolf, R.; Pieber, S. M.; Bruns, E. A.; Crippa, M.; Ciarelli, G.; Piazzalunga, A.; Schwikowski, M.; Abbaszade, G.; Schnelle-Kreis, J.; Zimmermann, R.; An, Z.; Szidat, S.; Baltensperger, U.; Haddad, I. E.; Prévôt, A. S. H. High secondary aerosol contribution to particulate pollution during haze events in China. *Nature* **2014**, *514* (7521), 218−22.

(2) Sun, X.; Zong, Z.; Wang, K.; Li, B.; Fu, D.; Shi, X.; Tang, B.; Lu, L.; Thapa, S.; Qi, H.; Tian, C. The importance of coal combustion and heterogeneous reaction for atmospheric nitrate pollution in a cold metropolis in China: Insights from isotope fractionation and Bayesian mixing model. *Atmos. Environ.* **2020**, *243*, No. 117730.

(3) Fan, M. Y.; Zhang, Y. L.; Lin, Y. C.; Hong, Y.; Zhao, Z. Y.; Xie, F.; Du, W.; Cao, F.; Sun, Y.; Fu, P. Important Role of NO_3 Radical to Nitrate Formation Aloft in Urban Beijing: Insights from Triple Oxygen Isotopes Measured at the Tower. *Environ. Sci. Technol.* **2022**, *56* (11), 6870−6879.

(4) Li, J.; Ho, S. C. H.; Griffith, S. M.; Huang, Y.; Cheung, R. K. Y.; Hallquist, M.; Hallquist, A. M.; Louie, P. K. K.; Fung, J. C. H.; Lau, A. K. H.; Yu, J. Z. Concurrent measurements of nitrate at urban and

suburban sites identify local nitrate formation as a driver for urban episodic $PM_{2.5}$ pollution. *Sci. Total Environ.* **2023**, *897*, No. 165351.
(5) Li, H.; Zhang, Q.; Zheng, B.; Chen, C.; Wu, N.; Guo, H.; Zhang, Y.; Zheng, Y.; Li, X.; He, K. Nitrate-driven urban haze pollution during summertime over the North China Plain. *Atmospheric Chemistry and Physics* **2018**, *18* (8), 5293−5306.
(6) Chan, Y.; Evans, M. J.; He, P.; Holmes, C. D.; Jaeglé, L.; Kasibhatla, P.; Liu, X.; Sherwen, T.; Thornton, J. A.; Wang, X.; Xie, Z.; Zhai, S.; Alexander, B. Heterogeneous Nitrate Production Mechanisms in Intense Haze Events in the North China Plain. *J. Geophys. Res.: Atmos.* **2021**, *126* (9), No. e2021JD034688.
(7) Wang, Y.; Liu, J.; Jiang, F.; Chen, Z.; Wu, L.; Zhou, S.; Pei, C.; Kuang, Y.; Cao, F.; Zhang, Y.; Fan, M.; Zheng, J.; Li, J.; Zhang, G. Vertical measurements of stable nitrogen and oxygen isotope composition of fine particulate nitrate aerosol in Guangzhou city: Source apportionment and oxidation pathway. *Sci. Total Environ.* **2023**, *865*, No. 161239.
(8) Zheng, B.; Zhang, Q.; Zhang, Y.; He, K. B.; Wang, K.; Zheng, G. J.; Duan, F. K.; Ma, Y. L.; Kimoto, T. Heterogeneous chemistry: a mechanism missing in current models to explain secondary inorganic aerosol formation during the January 2013 haze episode in North China. *Atmospheric Chemistry and Physics* **2015**, *15* (4), 2031−2049.
(9) He, P.; Xie, Z.; Chi, X.; Yu, X.; Fan, S.; Kang, H.; Liu, C.; Zhan, H. Atmospheric $\Delta^{17}O(NO_3^-)$ reveals nocturnal chemistry dominates nitrate production in Beijing haze. *Atmospheric Chemistry and Physics* **2018**, *18* (19), 14465−14476.
(10) Cao, Y.; Ma, Q.; Chu, B.; He, H. Homogeneous and heterogeneous photolysis of nitrate in the atmosphere: state of the science, current research needs, and future prospects. *Front. Environ. Sci. Eng* **2023**, *17* (4), 48.
(11) Brown, S. S.; Dubé, W. P.; Peischl, J.; Ryerson, T. B.; Atlas, E.; Warneke, C.; de Gouw, J. A.; te Lintel Hekkert, S.; Brock, C. A.; Flocke, F.; Trainer, M.; Parrish, D. D.; Feshenfeld, F. C.; Ravishankara, A. R. Budgets for nocturnal VOC oxidation by nitrate radicals aloft during the 2006 Texas Air Quality Study. *J. Geophys. Res.: Atmos.* **2011**, *116*, n/a.
(12) Song, W.; Liu, X.; Liu, C. New Constraints on Isotopic Effects and Major Sources of Nitrate in Atmospheric Particulates by Combining $\delta^{15}N$ and $\Delta^{17}O$ Signatures. *J. Geophys. Res.: Atmos.* **2021**, *126* (16), No. e2020JD034168.
(13) Zhang, Y. L.; Zhang, W.; Fan, M. Y.; Li, J.; Fang, H.; Cao, F.; Lin, Y. C.; Wilkins, B. P.; Liu, X.; Bao, M.; Hong, Y.; Michalski, G. A diurnal story of $\Delta^{17}O(NO_3^-)$ in urban Nanjing and its implication for nitrate aerosol formation. *npj Climate and Atmospheric Science* **2022**, *5*, 50.
(14) Zhang, Z.; Zheng, N.; Liang, Y.; Luo, L.; Xiao, H.; Xiao, H. Dominance of Heterogeneous Chemistry in Summertime Nitrate Accumulation: Insights from Oxygen Isotope of Nitrate ($\delta^{18}O$-NO_3^-). *Acs Earth and Space Chemistry* **2020**, *4* (6), 818−824.
(15) Zong, Z.; Tan, Y.; Wang, X.; Tian, C.; Li, J.; Fang, Y.; Chen, Y.; Cui, S.; Zhang, G. Dual-modelling-based source apportionment of NOx in five Chinese megacities: Providing the isotopic footprint from 2013 to 2014. *Environ. Int.* **2020**, *137*, 105592−105592.
(16) Zhao, Z.-Y.; Cao, F.; Fan, M.-Y.; Zhai, X.-Y.; Yu, H.-R.; Hong, Y.; Ma, Y.-J.; Zhang, Y.-L. Nitrate aerosol formation and source assessment in winter at different regions in Northeast China. *Atmos. Environ.* **2021**, *267*, No. 118767.
(17) Xiao, H.; Zhu, R.; Pan, Y.; Guo, W.; Zheng, N.; Liu, Y.; Liu, C.; Zhang, Z.; Wu, J.; Kang, C.; Luo, L.; Xiao, H. Differentiation Between Nitrate Aerosol Formation Pathways in a Southeast Chinese City by Dual Isotope and Modeling Studies. *J. Geophys. Res.: Atmos.* **2020**, *125* (13), No. e2020JD032604.
(18) Chang, Y.; Zhang, Y.; Tian, C.; Zhang, S.; Ma, X.; Cao, F.; Liu, X.; Zhang, W.; Kuhn, T.; Lehmann, M. F. Nitrogen isotope fractionation during gas-to-particle conversion of NOx to NO_3^- in the atmosphere − implications for isotope-based NOx source apportionment. *Atmospheric Chemistry and Physics* **2018**, *18* (16), 11647−11661.
(19) Zong, Z.; Tian, C.; Li, J.; Syed, J. H.; Zhang, W.; Fang, Y.; Jiang, Y.; Nasir, J.; Mansha, M.; Rizvi, S. H. H.; Shafiq, M.; Farhan, S. B.; Zhang, G. Isotopic Interpretation of Particulate Nitrate in the Metropolitan City of Karachi, Pakistan: Insight into the Oceanic Contribution to NOx. *Environ. Sci. Technol.* **2020**, *54* (13), 7787−7797.
(20) Zong, Z.; Tan, Y.; Wang, X.; Tian, C.; Fang, Y.; Chen, Y.; Fang, Y.; Han, G.; Li, J.; Zhang, G. Assessment and quantification of NOx sources at a regional background site in North China: Comparative results from a Bayesian isotopic mixing model and a positive matrix factorization model. *Environ. Pollut.* **2018**, *242* (Pt B), 1379−1386.
(21) He, P.; Xie, Z.; Yu, X.; Wang, L.; Kang, H.; Yue, F., The observation of isotopic compositions of atmospheric nitrate in Shanghai China and its implication for reactive nitrogen chemistry. *Sci. Total Environ.* **2020**, *714*, 136727.
(22) Li, Z.; Walters, W. W.; Hastings, M. G.; Song, L.; Huang, S.; Zhu, F.; Liu, D.; Shi, G.; Li, Y.; Fang, Y. Atmospheric nitrate formation pathways in urban and rural atmosphere of Northeast China: Implications for complicated anthropogenic effects. *Environ. Pollut.* **2022**, *296*, No. 118752.
(23) Song, W.; Liu, X.-Y.; Wang, Y.-L.; Tong, Y.-D.; Bai, Z.-P.; Liu, C.-Q. Nitrogen isotope differences between atmospheric nitrate and corresponding nitrogen oxides: A new constraint using oxygen isotopes. *Sci. Total Environ.* **2020**, *701*, No. 134515.
(24) Feng, S.; Xu, W.; Cheng, M.; Ma, Y.; Wu, L.; Kang, J.; Wang, K.; Tang, A.; Collett, J. L.; Fang, Y.; Goulding, K.; Liu, X.; Zhang, F. Overlooked Nonagricultural and Wintertime Agricultural NH_3 Emissions in Quzhou County, North China Plain: Evidence from ^{15}N-Stable Isotopes. *Environmental Science & Technology Letters* **2022**, *9* (2), 127−133.
(25) Feng, X.; Chen, Y.; Du, H.; Feng, Y.; Mu, Y.; Chen, J. Biomass Burning is a Non-negligible Source for Ammonium During Winter Haze Episodes in Rural North China: Evidence From High Time Resolution ^{15}N-stable Isotope. *J. Geophys. Res.: Atmos.* **2023**, *128* (3), No. e2022JD03801.
(26) Zhang, Y.; Zhao, Z.; Cao, F.; Song, W.; Lin, Y.; Fan, M.; Yu, H.; Li, H.; Hong, Y.; Gao, M. Changes in atmospheric oxidants over Arctic Ocean atmosphere: evidence of oxygen isotope anomaly in nitrate aerosols. *npj Clim. Atmos. Sci.* **2023**, *6* (1), 1−9.
(27) Thiemens, M. H. Mass-Independent Isotope Effects in Planetary Atmospheres and the Early Solar System. *Science* **1999**, *283*, 341−345.
(28) Albertin, S.; Savarino, J.; Bekki, S.; Barbero, A.; Caillon, N. Measurement report: Nitrogen isotopes ($\delta^{15}N$) and first quantification of oxygen isotope anomalies ($\Delta^{17}O$, $\delta^{18}O$) in atmospheric nitrogen dioxide. *Atmospheric Chemistry and Physics* **2021**, *21* (13), 10477−10497.
(29) Alexander, B.; Hastings, M. G.; Allman, D. J.; Dachs, J.; Thornton, J. A.; Kunasek, S. A. Quantifying atmospheric nitrate formation pathways based on a global model of the oxygen isotopic composition ($\Delta^{17}O$) of atmospheric nitrate. *Atmos. Chem. Phys.* **2009**, *9*, 5043−5056.
(30) Michalski, G.; Bhattacharya, S. K.; Mase, D. F.; Baskaran, M. Mase, Oxygen Isotope Dynamics of Atmospheric Nitrate and Its Precursor Molecules. *Handbook Environ. Isotope Geochem.* **2011**, *30*, 613−634.
(31) Fan, M.-Y.; Zhang, Y.-L.; Lin, Y.-C.; Chang, Y.-H.; Cao, F.; Zhang, W.-Q.; Hu, Y.-B.; Bao, M.-Y.; Liu, X.-Y.; Zhai, X.-Y.; Lin, X.; Zhao, Z.-Y.; Song, W.-H. Isotope-based source apportionment of nitrogen-containing aerosols: A case study in an industrial city in China. *Atmos. Environ.* **2019**, *212*, 96−105.
(32) Zong, Z.; Wang, X.; Tian, C.; Chen, Y.; Fang, Y.; Zhang, F.; Li, C.; Sun, J.; Li, J.; Zhang, G. First Assessment of NOx Sources at a Regional Background Site in North China Using Isotopic Analysis Linked with Modeling. *Environ. Sci. Technol.* **2017**, *51* (11), 5923−5931.
(33) Fang, Y. T.; Koba, K.; Wang, X. M.; Wen, D. Z.; Li, J.; Takebayashi, Y.; Liu, X. Y.; Yoh, M. Anthropogenic imprints on nitrogen and oxygen isotopic composition of precipitation nitrate in a

nitrogen-polluted city in southern China. *Atmospheric Chemistry and Physics* **2011**, *11* (3), 1313−1325.
(34) Johnston, J. C.; Thiemens, M. H. The isotopic composition of tropospheric ozone in three environments. *Journal of Geophysical Research-Atmospheres* **1997**, *102* (D21), 25395−25404.
(35) Krankowsky, D.; Bartecki, F.; Klees, G. G.; Mauersberger, K.; Schellenbach, K.; Stehr, J. Measurement of heavy isotope enrichment in tropospheric ozone. *Geophys. Res. Lett.* **1995**, *22* (13), 1713−1716.
(36) Morin, S.; Sander, R.; Savarino, J. Simulation of the diurnal variations of the oxygen isotope anomaly ($\Delta^{17}O$) of reactive atmospheric species. *Atmospheric Chemistry and Physics* **2011**, *11* (8), 3653−3671.
(37) Alexander, B.; Sherwen, T.; Holmes, C. D.; Fisher, J. A.; Chen, Q.; Evans, M. J.; Kasibhatla, P. Global inorganic nitrate production mechanisms: comparison of a global model with nitrate isotope observations. *Atmos. Chem. Phys.* **2020**, *20*, 3859−3877.
(38) Kunasek, S. A.; Alexander, B.; Steig, E. J.; Hastings, M. G.; Gleason, D. J.; Jarvis, J. C. Measurements and modeling of $\Delta^{17}O$ of nitrate in snowpits from Summit, Greenland. *J. Geophys. Res.: Atmos.* **2008**, *113*, D24302.
(39) Kanaya, Y.; Fukuda, M.; Akimoto, H.; Takegawa, N.; Komazaki, Y.; Yokouchi, Y.; Koike, M.; Kondo, Y. Urban photochemistry in central Tokyo: 2. Rates and regimes of oxidant (O_3+NO_2) production. *J. Geophys. Res.: Atmos.* **2008**, *113*, D06301.
(40) Song, M.; Liu, X.; Tan, Q.; Feng, M.; Qu, Y.; An, J.; Zhang, Y. Characteristics and formation mechanism of persistent extreme haze pollution events in Chengdu, southwestern China. *Environ. Pollut.* **2019**, *251*, 1−12.
(41) Shi, P.; Zhang, G.; Kong, F.; Chen, D.; Azorin-Molina, C.; Guijarro, J. A. Variability of winter haze over the Beijing-Tianjin-Hebei region tied to wind speed in the lower troposphere and particulate sources. *Atmospheric Research* **2019**, *215*, 1−11.
(42) Liu, C.; Hua, C.; Zhang, H.; Zhang, B.; Wang, G.; Zhu, W.; Xu, R. A severe fog-haze episode in Beijing-Tianjin-Hebei region: Characteristics, sources and impacts of boundary layer structure. *Atmospheric Pollution Research* **2019**, *10* (4), 1190−1202.
(43) Feng, X.; Feng, Y.; Chen, Y.; Cai, J.; Li, Q.; Chen, J. Source apportionment of $PM_{2.5}$ during haze episodes in Shanghai by the PMF model with PAHs. *Journal of Cleaner Production* **2022**, *330*, No. 129850.
(44) Guha, T.; Lin, C. T.; Bhattacharya, S. K.; Mahajan, A. S.; Ou-Yang, C.-F.; Lan, Y.-P.; Hsu, S. C.; Liang, M.-C. Isotopic ratios of nitrate in aerosol samples from Mt. Lulin, a high-altitude station in Central Taiwan. *Atmos. Environ.* **2017**, *154*, 53−69.
(45) Lu, K.; Fuchs, H.; Hofzumahaus, A.; Tan, Z.; Wang, H.; Zhang, L.; Schmitt, S. H.; Rohrer, F.; Bohn, B.; Broch, S.; Dong, H.; Gkatzelis, G. I.; Hohaus, T.; Holland, F.; Li, X.; Liu, Y.; Liu, Y.; Ma, X.; Novelli, A.; Schlag, P.; Shao, M.; Wu, Y.; Wu, Z.; Zeng, L.; Hu, M.; Kiendler-Scharr, A.; Wahner, A.; Zhang, Y. Fast Photochemistry in Wintertime Haze: Consequences for Pollution Mitigation Strategies. *Environ. Sci. Technol.* **2019**, *53* (18), 10676−10684.
(46) Rohrer, F.; Berresheim, H. Strong correlation between levels of tropospheric hydroxyl radicals and solar ultraviolet radiation. *Nature* **2006**, *442* (7099), 184−187.
(47) Wang, Y.-L.; Song, W.; Yang, W.; Sun, X.-C.; Tong, Y.-D.; Wang, X.-M.; Liu, C.-Q.; Bai, Z.-P.; Liu, X.-Y. Influences of Atmospheric Pollution on the Contributions of Major Oxidation Pathways to $PM_{2.5}$ Nitrate Formation in Beijing. *Journal of Geophysical Research-Atmospheres* **2019**, *124* (7), 4174−4185.
(48) Liu, S.; Liang, X.-Z. Observed Diurnal Cycle Climatology of Planetary Boundary Layer Height. *Journal of Climate* **2010**, *23* (21), 5790−5809.
(49) Dubey, M. K.; Mohrschladt, R.; Donahue, N. M.; Anderson, J. G. Isotope Specific Kinetics of Hydroxyl Radical (OH) with Water (H_2O): Testing Models of Reactivity and Atmospheric Fractionation. *J. Phys. Chem. A* **1997**, *101*, 1494−1500.
(50) Carslaw, N.; Creasey, D. J.; Heard, D. E.; Lewis, A. C.; McQuaid, J. B.; Pilling, M. J.; Monks, P. S.; Bandy, B. J.; Penkett, S. A. HO_2, and RO_2 radicals in the marine boundary layer: 1. Model construction and comparison with field measurements. *J. Geophys. Res.: Atmos.* **1999**, *104* (D23), 30241−30255.

https://doi.org/10.1021/acs.est.3c07590
Environ. Sci. Technol. 2023, 57, 20726−20735